Synthesis of Bis (Benzoyl Acetone Ethylene Diimine) Schiff Base Complex of Nickel (II) Supported on Magnetite Silica Nano-Particles (Fe_3O_4@Sio_2/Schiff-Base Of Ni (II)) and Using it as an Efficient Catalyst for Green Synthesis of 1-Amidoalkyl-2-Naphthol.

Moslem Setoodehkhah (setoodehkhah@kashanu.ac.ir)
University of Kashan https://orcid.org/0000-0002-3739-6841
Amin Mazraati
University of Kashan
Mohsen Moradian
University of Kashan

Research Article

Keywords: Bis (benzoyl acetone ethylenediimine), Schiff-base, Magnetite nanoparticles, core-shell, 1-Amidoalkyl-2-naphthol, green synthesis

Posted Date: July 15th, 2021

DOI: https://doi.org/10.21203/rs.3.rs-700894/v1

Abstract

In this research, magnetite nano-particles as the core are fabricated by co-precipitation method from Fe(II) and Fe(III) chloride salts and then the surfaces of the nano-particles are modified to improve their performance. These modifications include the coating of silica and then the second layer by 3-amino propyl triethoxy silane (APTES) which causes the functionalization of magnetite nanoparticles with $-NH_2$ groups. In the next step, an aliphatic tetra-dentate N_2O_2 Schiff base was synthesized by condensation reaction between benzoyl acetone and ethylenediamine. Then this Schiff base is immobilized on the magnetite silica surfaces. This immobilized Schiff base was converted to the Ni (II) Schiff base complex by the reaction with Ni(II) acetate tetrahydrate. This Ni (II) Schiff base complex is immobilized on magnetite silica and shown as Fe_3O_4@SiO_2/Schiff base of Ni (II). This cor-shell nano-structure is fully characterized by techniques such as FT-IR, VSM, XRD, FE-SEM, EDX, TGA-DTA, AAS, BET, and BJH. In the last step, this nano-catalyst is used as an efficient catalyst for the solvent-free synthesis of amido alkyl naphthols by the condensation reaction between an aldehyde, 2-naphthol, and an amide. The reaction was monitored by TLC. At the end of the reaction, the nano-catalyst was removed easily from the reaction mixture by an external magnet. The products of amido alkyl naphthols were identified by FT-IR and ^{1}HNMR techniques. Finally, the percentage yield of the reaction is calculated by measuring the mass of 1-amidoalkyl-2-naphthol synthesized in the presence of the catalyst.

1 Introduction

In recent years, the synthesis of Magnetic nanoparticles (MNPs) have advantages and make higher interest and attention because of their properties and potential applications in different fields [1] for example catalyst [2], drug delivery systems [3, 4], and cancer treatments [5]. Magnetite iron oxide nano-particles especially Fe_3O_4 are very well known for researchers because of their special physical properties including low toxicity [6], high surface area [7, 8] easy preparation, and easy recycling with a simple external magnet [9]. Preparation of magnetic core-shell nano-catalyst with Fe_3O_4 spheres as the core and organic or inorganic materials such as SiO_2 which is used as the shell is very common [10, 11]. The surface of core-shell MNPs is hydrophilic with silica and is modified easily with various functional groups [12, 13]. 3-Aminopropyltriethoxysilane (APTES) can be a modifier of nano core-shell surface (Fe_3O_4@ SiO_2/ APTES) [14, 15]. In recent decade, the Schiff base especially imine structures as chelating ligand plays a prominent role in organic and inorganic chemistry [16]. They also have an important role in transition metal coordination chemistry [17, 18]. The advantages of these ligands are that they make a stable complex with the most transition metals and have the great efficiency as catalyst [19, 20]. But the extraction of these catalysts from the reactions is difficult for the chemist.

Schiff base ligands and complexes can be used for functinalization of magnetic cores such as magnetite silica. These core-shell structures can be used as catalyst in organic reactions and at the end of the reaction, the catalyst is easily extracted from the reaction mixture by an external magnet. Synthesis,

characterization and various applications of Schiff bases functinalized different matrices such as magnetic cores are the subject of several studies [21–24].

The synthesis of 1-Amidoalkyl-2-naphthols is one of the multi-component reactions [25]. The advantages of this method are decreasing reaction time and saving energy [26]. In recent years, researchers have made great efforts to find and expand new MCRs [27]. 1-amidoalkyl-2-naphthols are very common to various biological importance in natural products [28]. Amidoalkyl-2-naphthols are effective medicine [29], including a number of nucleoside antibiotic [30] and HIV protease inhibitor [31] such as lopinavir, antibacterial [32], anti-inflammatory [33], bradycardia activities and hypotensive [34]. The anticancer activities of these compounds have also been evaluated [35]. The derivation of these products has made interest because of their pharmaceutical activities [36, 37] For example; 1-amido-alkyl-2-naphthols have been reported to show cardiovascular activity [38]. The hypertensive effect of these compounds is very familiar for researchers [39]. The preparation and synthesis of 1-amidoalkyl-2-naphthol derivations can be carried out by multi-components condensation of most from aromatic and some aliphatic aldehyde, 2-naphthol, and also amide group in the presence of Lewis acid catalysts such as iodine, $FeCl_3$, etc have been reported [40, 41]. However, some of these methods have disadvantages such as long reaction time, higher reaction temperature (> 100 ˚C), low product yield, using of toxin and dangerous solvent that is very harmful to the environment [42].

In this work, a novel catalyst, Fe_3O_4@SiO_2/Schiff base of Ni (II), was synthesized and characterized. In this core-shell structure, an aliphatic Schiff base is supported on magnetite nano-particles and used as an efficient catalyst for the synthesis of 1-amidoalkyl-2-naphthol derivations in solvent-free conditions.

2 Experimental

2.1 Chemical and instrumentations

All chemical materials were obtained from Merck and Fluka and used without further purification. ^{1}HNMR spectra were recorded with Bruker advance DPX 400 MHz spectrometer in DMSO-d6 as a solvent in the presence of TMS for the internal standard. Fourier transform infrared (FT-IR) spectra were recorded as KBr pellets using a Perkin-Elmer 781 spectrophotometer. X-ray powder diffraction (XRD patterns of samples) was obtained with a Philips X-ray powder diffractometer (CuKα radiation, λ = 0.154056 nm). Field emission scanning electron microscopy (FE-SEM) images were obtained on Zeiss XL-30ESEM. Atomic absorption spectrophotometer (AAS), were obtained with Perkin-Elmer 2380. The vibrating sample magnetometer (VSM) by Maghnetis daghigh kavir Co was used to research the magnetite parameter thermogravimetric analysis. TGA-DTA curves were recorded by a Rheometric Scientific Inc 1998 thermal analysis apparatus under an N_2 atmosphere. BET & BJH curves were used for measurement of nano-catalyst specific surface area with ISO15901-2 model numbers.

2.2 Synthesis of Fe_3O_4 as nanoparticle

Magnetite nano-particles were synthesized by a method described previously [10]. Briefly, 6.0 g (0.022 mole) of $FeCl_3.6H_2O$ salt in 30 mL water was added to 3.0 g (0.011 mole) $FeCl_2.4H_2O$ salt in 20 mL water. The solution was stirred mechanically at room temperature for 20 min. and then this mixture was stirred at 70 ˚C for half an hour (30 min.). In this condition ammonia solution (25%) was added to pH is fixed at 10. At this time, the black sediment of magnetite was formed and then the mixture stirred for 1 hour at 60˚C. Finally, the product was extracted by an external magnet and washed three times with deionized water, and dried under vacuum at 65˚C.

2.3 Synthesis of $Fe_3O_4@SiO_2$ core-shell

The $Fe_3O_4@SiO_2$ core-shell was synthesized by some modification of the Stober method [11]. In short, 0.5 g of synthesized magnetite nano-particles was dispersed in a mixture of 5 mL deionized water and 50 mL ethanol. Then, 0.2 mL TEOS and 5 mL NaOH (10% w) were added to the mentioned mixture. The mixture was stirred mechanically at room temperature for 70 min. Then the dark brown core-shell product ($Fe_3O_4@SiO_2$) is formed. This product removed by an external magnet, washed three times with deionized water and ethanol, and dried at 90˚C for 12 hours.

2.4 Preparation of $Fe_3O_4@SiO_2$/APTES

$Fe_3O_4@SiO_2$/APTES was prepared according to the previously reported procedure [14]. Briefly, 0.2 g of dark brown core-shell ($Fe_3O_4@SiO_2$) was added to 0.2 mL APTES in 4.8 mL dry toluene and then this mixture was dispersed by ultrasonic for 20 min. The mixture refluxed for 24 hours at 110–120˚C. After the mixture was cooled to room temperature, the precipitate was collected by an external magnet. The product was washed three times with water, toluene, and ethanol and was dried at 90˚C. The color of this product was dark brown too.

2.5 Synthesis of Schiff base (bis (benzoyl acetone ethylene diimine)) (BBE)

The synthesis of the Schiff base ligand was used in this work and was done according to the previously reported [16]. In short, a mixture of 2 mmole anhydrous ethylenediamine in 20 mL methanol was added gradually (dropwise) to a solution of 4 mmole benzoyl acetone in 50 mL methanol for 5 hours at room temperature. During this time a white precipitate was formed. The reaction mixture was stirred for an additional hour and filtered. The crystal of the product was washed three times with ethanol and recrystallized in methanol. Finally, the crystal of Bis (benzoyl aceton) ethylene diimine (BBE) dried in a vacuum at 80˚C for 12 hours. At room temperature, this Schiff base ligand is insoluble in water but is soluble in common organic solvents. The synthesis of BBE has been shown in Scheme 1.

2.6 Preparation of $Fe_3O_4@SiO_2$ /Schiff base

1mmole of BBE Schiff base ligand was dissolved in 20 mL ethanol and then was added to 0.5 g $Fe_3O_4@SiO_2$/APTES in 30 mL ethanol. This mixture was dispersed in ultrasonic for 20 min and then

refluxed for 24 hours in 110–120˚C. After cooling the mixture the solid product was extracted easily by an external powerful magnet and washed three times with ethanol and finally was dried at 80˚C for 8 hours.

2.7 Synthesis of Fe_3O_4@SiO_2/ Schiff base of Ni (II) (MSA-SB@Ni (II))

0.3 g of Fe_3O_4@SiO_2/Schiff base was dispersed in 15 mL of ethanol by using ultrasonic for until the particles were diffused in solution (20 min.). 0.15 g (0.85 mmole) salt of nickel (II) acetate tetrahydrate (Ni $(CH_3COO)_2.4H_2O$) as the source of Ni(II) ion, was added dropwise to the mixture. The mixture was refluxed for 24 hours in 110˚C. Then the solid product was separated by a powerful external magnet and washed three times with deionized water and ethanol. Finally, the Fe_3O_4@SiO_2/Schiff base of Ni (II) catalyst dried under vacuum at 80˚C for 12 hours. The preparation of nano-catalyst (MSA-SB@Ni (II)) has been shown step by step at Scheme 1.

2.8 Synthesis of Amidoalkyl-2-naphthol as our main purpose

As every chemist knows, there are many methods to prepare this essential compound but our work introduces one of the best methods for synthesizing amido alkyl-2-naphthol. The catalyst is separated easily by an external magnet. The catalyst Fe_3O_4@SiO_2/Schiff base of Ni (II) (MSA-SB@Ni) was added to a mixture of 1mmole aromatic aldehyde, 1mmole 2-naphthol, and 1.5mmole amide and stirred in 80–90˚C for 180 min. During this time the product was formed. TLC, ^{1}HNMR, FT-IR confirmed our claim (Scheme 2).

2.9 Spectroscopic and physical data

N-[phenyl-(2-hydroxy-naphthalen-1-yl)-methyl]-acetamide

Yield: 92%, milky solid, mp: 240–242˚C, IR (KBr), v (cm^{-1}): 3400.48 (O-H, Ar, str, vib), 3249.97 (N-H of amide, str), 3060 (C-H, Ar, str), 1639.06 (> C=O, amide, str), 1516 – 1436 (C=C, Ar, str), 1274 – 1063 (C-N/C-O, str), 809 (C-H, Ar, out of plane, bend), 743.14 (N-H, out of plane bend). ^{1}HNMR (400 MHz, DMSO – d_6 / TMS) σ (ppm): 1.97–2.07 (s, 3H), 7.06 (d, *J = 8.*1 Hz, 1H), 7.10 (d, *J = 8.6* Hz, 2H), 7.12 (d, *J = 8.6* Hz, 1H), 7.14 (m, 3H), 7.15 (t, *J = 7.5* Hz, 1H), 7.23 (m, 3H), 7.38 (d, *J = 8.6* Hz, 1H), 9.98 (s, 1H). 2.49 (DMSO), 3.34 (HDO).

N-[(2-chloro-phenyl)-(2-hydroxy-naphthalen-1-yl)-methyl]-acetamide

Yield: 93%, white solid, m.p: 213–216˚C, IR (KBr), v (cm^{-1}): 3419.29 (N-H of amide, str) ,3227.04 (O-H, Ar, str, vib), 3050 (C-H, Ar, str), 1641.05 (> C=O, amide, str), 1514 – 1438 (C=C, Ar, str), 1270.3-1060.7(C-N/C-O, str), 812.57 (C-H, Ar, out of plane, bend),749.40 (N-H, out of plane bend) ^{1}HNMR (400 MHz, DMSO – d_6/TMS) σ (ppm): 1.91–2.07 (s, 3H), 7-7.06 (d, *J = 8.*2 Hz, 1H), 7.11 (d, *J = 8.6* Hz, 2H), 7.18 (d, *J = 8.6* Hz,

1H), 7.20 (m, 3H), 7.31 (t, *J = 7.5* Hz, 1H), 7.73 (m, 3H), 8.42 (d, *J = 8.6* Hz, 1H), 10.09 (s, 1H). 2.49 (DMSO), 3.34 (HDO).

N -[(3-nitro-phenyl)-(2-hydroxy-naphthalen-1-yl)-methyl]-acetamide

Yield: 95%, yellow solid, m.p: 253–256˚C, IR (KBr), v (cm^{-1}): 3452.66 (O-H, Ar, str, vib), 3147.59 (N-H of amide, str), 3022 (C-H, Ar, str), 1688.84 (> C=O, amide, str), 1519.91–1400 (C=C, Ar, str), 1259 – 1167 (C-N/C-O, str), 810 (C-H, Ar, out of plane, bend), 747.46 (N-H, out of plane bend). ^{1}H NMR (400MHz, DMSO – d_6/TMS) σ (ppm): 2.06 (s, 3H), 6.53 (t, J = 8.0 Hz, 1H), 7.07 (d, J = 8.6 Hz, 1H), 7.22 (t, J = 7.5 Hz, 1H), 7.34 (t, J = 7.4 Hz, 1H), 7.58 (m, 2H), 7.63 (t, J = 8.6 Hz, 2H), 7.72 (br, 1H), 8.33 (m, 2H), 9.12 (d, J = 8.0 Hz, 1H), 9.66 (s, 1H) ppm. 2.47 (DMSO), 3.31 (HDO).

N -[(3-hydroxy-phenyl)-(2-hydroxy-naphthalen-1-yl)-methyl]-acetamide

Yield: 88%, milky solid, m.p: 224–227˚C, IR (KBr), v (cm^{-1}): 3372.53 (O-H, Ar, str, vib), 3200 (N-H of amide,str), 3020 (C-H, Ar, str), 1629 (> C=O, amide, str), 1512 – 1461 (C=C, Ar, str), 1276-1170.7 (C-N/C-O, str), 814.57 (C-H, Ar, out of plane,bend), 743.28(N-H, out of plane bend). ^{1}H NMR (400MHz, DMSO – d_6/TMS) σ (ppm): 2.06 (s, 3H), 7.06 (t, J = 8.0 Hz, 1H), 7.08 (d, J = 8.6 Hz, 1H), 7.22 (t, J = 7.5 Hz, 1H), 7.34 (t, J = 7.4 Hz, 1H), 7.67 (m, 2H), 7.71 (t, J = 8.6 Hz, 2H), 8.13 (br, 1H), 8.15 (m, 2H), 8.30 (d, J = 8.0 Hz, 1H), 9.66 (s, 1H) ppm. 2.64(DMSO), 3.31 (HDO).

N -[(2,4-Dihydroxy-phenyl)-(2-hydroxy-naphthalen-1-yl)-methyl]-acetamide

Yield: 86%, red solid, m.p: 228–230 ˚C IR (KBr), v (cm^{-1}): 3417.40 (N-H of amide, str), 2923 – 2853 (C-H, Ar, str), 1627.22(> C=O, amide, str), 1510 – 1461(C=C, Ar, str),1219 – 1170 (C-N/C-O, str), 812.89 (C-H, Ar, out of plane,bend),745.64 (N-H,out of plane bend). ^{1}H NMR (400MHz, DMSO – d_6/TMS) σ (ppm): 2.05 (s, 3H), 7.06 (t, J = 8.0 Hz, 1H), 7.22 (d, J = 8.6 Hz, 1H), 7.34 (t, J = 7.5 Hz, 1H), 7.63(t, J = 7.4 Hz, 1H), 7.71 (m, 2H), 8.13 (t, J = 8.6 Hz, 2H), 8.15 (br, 1H), 8.30 (m, 2H), 9.65 (d, J = 8.0 Hz, 1H), 9.66 (s, 1H) ppm. 2.62 (DMSO), 3.31 (HDO).

N -[(2-bromo 5-hydroxy-phenyl)-(2-hydroxy-naphthalen-1-yl)-methyl]-acetamide

Yield: 93%, white solid, m.p: 273–275 ˚C .IR (KBr), v (cm^{-1}): 3390 (O-H, Ar, str, vib), 3242 (N-H of amide, str), 2970-2870.39 (C-H, Ar, str), 1668.34 (> C=O, amide, str), 1515 – 1465 (C=C, Ar, str), 1270 – 1263 (C-N/C-O, str), 827 (C-H, Ar, out of plane,bend), 761 (N-H,out of plane bend). ^{1}HNMR (400MHz, DMSO – d_6/TMS) σ (ppm): 2.48 (s, 3H), 7.06 (t, J = 8.0 Hz, 1H), 7.09 (d, J = 8.6 Hz, 1H), 7.22 (t, J = 7.4 Hz, 1H), 7.24 (t, J = 7.5 Hz, 1H), 7.34 (m, 2H), 7.67 (t, J = 8.6 Hz, 2H), 7.95 (br, 1H), 8.15 (m, 2H), 8.33 (d, J = 8.0 Hz, 1H), 9.68 (s, 1H) ppm. 2.62 (DMSO), 3.31 (HDO).

N -[(heptyle-(2-hydroxy-naphthalen-1-yl)-methyl]-acetamide

Yield: 90%, milky solid, m.p: 224 ˚C IR (KBr), v (cm^{-1}): 3415 (O-H, Ar, str, vib), 3196 (N-H of amide, str), 2926 (C-H, Ar, str), 1638 (> C=O, amide, str), 1536 (C=C, Ar, str), 1275 (C-N/C-O, str), 814 (C-H, Ar, out of plane,bend), 751 (N-H, out of plane bend). ^{1}H NMR (400MHz, DMSO – d_6/TMS) σ (ppm): 1.89 (s, 3H), 5.94 (t, J = 8.0 Hz, 1H), 7.10 (d, J = 8.6 Hz, 1H), 7.27 (t, J = 7.5 Hz, 1H), 7.42 (t, J = 7.4 Hz, 1H), 7.46 (m, 2H), 7.48 (t, J = 8.6 Hz, 2H), 7.78 (br, 1H), 8.30 (m, 2H), 9.71 (d, J = 8.0 Hz, 1H), 10.10 (s, 1H) ppm. 2.49 (DMSO), 3.37 (HDO).

N **-[(3-nitro-phenyl)-(2-hydroxy-naphthalen-1-yl)-phenyl]-urea**

Yield: 94%, light yellow solid, m.p: 191–193, IR (KBr), v (cm^{-1}): 3451.23 (O-H, Ar, str, vib), 3397 – 3310 (N-H of amide, str), 2924 (C-H, Ar, str), 1688.74 (> C=O, amide, str), 1518 – 1404 (C=C, Ar, str), 1257 – 1168 (C-N/C-O, str), 811.61 (C-H, Ar, out of plane, bend), 746 (N-H, out of plane bend). ^{1}HNMR (400MHz, DMSO – d_6/TMS) (ppm): 1.88 (s, 2H), 6.96 (t, J = 8.0 Hz, 1H), 7.08 (d, J = 8.6 Hz, 1H), 7.27 (t, J = 7.5 Hz, 1H), 7.35 (t, J = 7.4 Hz, 1H), 7.67 (m, 2H), 7.70 (t, J = 8.6 Hz, 2H), 8.15 (br, 1H), 9.68 (m, 2H), 10.19 (d, J = 8.0 Hz, 1H), 10.94 (s, 1H) ppm. 2.48 (DMSO), 3.31 (HDO).

N **-[(2,4-Dihydroxy-phenyl)-(2-hydroxy-naphthalen-1-yl)-phenyl]-urea**

Yield: 89%, red solid, m.p: 250–254. IR (KBr), v (cm^{-1}): 3405 (O-H, Ar, str, vib), 3212 (N-H of amide, str), 3054 (C-H, Ar, str), 1625 (> C=O, amide, str), 1509 (C=C, Ar, str), 1232 (C-N/C-O, str), 809 (C-H, Ar, out of plane, bend), 742 (N-H, out of plane bend). ^{1}H NMR (400 MHz, DMSO – d_6/TMS) σ (ppm): 2.06 (s, 3H), 5.77 (t, J = 8.0 Hz, 1H), 6.24 (d, J = 8.6 Hz, 1H), 6.29 (t, J = 7.5 Hz, 1H), 6.40 (t, J = 7.4 Hz, 1H), 7.04(m, 2H), 7.06 (t, J = 8.6 Hz, 2H), 7.09 (br, 1H), 7.20 (m, 2H), 7.29 (d, J = 8.0 Hz, 1H), 9.66 (s, 1H) ppm. 2.49 (DMSO), 3.38 (HDO).

N **-[(2,5-dimethoxy-phenyl)-(2-hydroxy-naphthalen-1-yl)-methyl]-acetamide**

Yield: 88%, milky solid, m.p: 250–252. IR (KBr), v (cm^{-1}): 3365 (O-H, Ar, str overlapping with N-H of amide, str), 3185 (C-H, Ar, str), 2900 – 2850 (C-H, alkane, str), 1643 (> C=O, amide, str), 1498 – 1434 (C=C, Ar, str), 1277 – 1054 (C-N/C-O, str), 818 (C-H, Ar, out of plane, bend), 751 – 726 (N-H, out of plane bend). ^{1}HNMR (400MHz, DMSO – d_6/TMS) σ (ppm): σ =1.87 (s, 3H), 3.32 (s, 3H), 3.46 (s, 3H), 6.69–6.77 (m, 2H), 7.10–7.24 (m, 4H), 7.39 (s, 1H), 7.66–7.73 (m, 2H), 8.15–8.29 (m, 2H), 9.77 (s, 1H) ppm. 2.49 (DMSO), 3.48 (HDO).

N **-[(3-nitro-phenyl)-(2-hydroxy-naphthalen-1-yl)-phenyl]-benzamide**

Yield: 92%, yellow solid, m.p: 214–217. IR (KBr), v (cm^{-1}): 3451.32 (O-H, Ar, str overlapping with N-H of amide, str), 3105 (C-H, Ar, str), 2900 (C-H, alkane, str), 1687.67 (> C=O, amide, str), 1517 (C=C, Ar, str), 1343 – 1258 (C-N/C-O, str), 853.56 (C-H, Ar, out of plane, bend), 747 (N-H, out of plane bend). ^{1}HNMR (400MHz, DMSO – d_6/TMS) σ (ppm): δ = 3.38 (s, 3H), 7.23–7.51 (m, 9H), 7.58 (d, J = 7.8 Hz, 1H), 7.81–7.90 (m, 4H), 8.08–8.31(m, 3H), 8.33 (d, J = 7.8 Hz, 1H), 9 .71(s, 1H).

3 Results And Discussion

3.1 Characterization of MSA-SB@Ni (nano-catalyst)

After successful synthesis of nano-catalyst, this compound fully characterized by various spectroscopic and microscopic techniques including FT-IR, TGA, VSM, XRD, SEM, AAS, EDX and BET respectively.

3.1.1 FT-IR spectra

The FT-IR spectra of bare Fe_3O_4 (MNPs) (a), $Fe_3O_4@SiO_2$ (b), $Fe_3O_4@SiO_2$/APTES (c), aliphatic tetra-dentate Schiff base (BBE) (d), $Fe_3O_4@SiO_2$/Schiff base (e), and MSA-SB@Ni (II) (f) have been shown in Fig. 1. The vibration bonds in the range of 568–574 cm^{-1} are assigned to the stretching vibrations of the "Fe – O" bond, these vibrations are common at all synthesized structures except free Schiff base ligand (Fig. 1. a, b, c, e, f). The vibration bonds that observed in the range of 1018–1100 cm^{-1} are assigned to symmetric and asymmetric "Si – O–Si" stretching. These bonds indicate that the silica-coated magnetite nano-particles have been synthesized successfully (Fig. 1. b, c, e and f (1018, 1034, 1048, 1040 cm^{-1} respectively). The bond at about 1650 cm^{-1} in $Fe_3O_4@SiO_2$/APTES (Fig. 1c) can be attributed to the "N – H" bending mode of the free NH_2 group. The vibration bonds at about 1650 and 1670 cm^{-1} in free Schiff base ligand (Fig. 1.d) can be assigned to "C = O"(carbonyl) and "C = N" (Imine) stretching which indicate synthesize of free Schiff base ligand [16]. The successful synthesis of Schiff base ligand supported on magnetite silica core-shell structure, was evidenced by comparison of the spectrum of free Schiff base ligand (Fig. 1d) and $Fe_3O_4@SiO_2$/Schiff base (Fig. 1e); The C = O stretching (1670 cm^{-1} in free Schiff base ligand) doesn't seen at spectrum of $Fe_3O_4@SiO_2$/Schiff base because of condensation reaction between C = O groups of free Schiff base ligand and $–NH_2$ groups of $Fe_3O_4@SiO_2$/APTES. The successful metalation of $Fe_3O_4@SiO_2$/Schiff base by Ni(II) was evidenced by the comparison of C = N stretching of Schiff base supported on magnetite silica (Fig. 1e) and MSA-SB@Ni(II) (Fig. 1f). The bond at 1652 cm^{-1} at spectrum of $Fe_3O_4@SiO_2$/Schiff base (Fig. 1e) is assigned to stretching of C = N, this bond at spectrum of MSA-SB@Ni(II) is seen at 1632 cm^{-1} (Fig. 1f) and shows 20 cm^{-1} red shift because of the coordination of Ni(II) ion to Schiff base ligand. The vibration bonds in the range 2923–3073 cm^{-1} corresponds to the stretching vibration of aromatic and aliphatic C-H bonds (Fig. 1c, d, e, f).

3.1.2 TGA-DTA curve

TGA was used to study the thermal stability of the novel catalyst (MSA-SB@Ni) and to estimate the thickness of silica layer magnetite and amount of Schiff base (BBE) attached to the surface of core-shell ($Fe_3O_4@SiO_2$). Figure 2 shows TGA curve of MSA-SB@Ni (II) It is very clear that, for the MSA-SB@Ni (II) MNPs, in the temperature range of 50 to 240˚C the weight loss of nanocomposite is about only 4% which can be referred to the loss of water that trapped in the catalyst. At 245 to 600˚C, the second step of weight loss was occurred which can be related to the decomposition of the Schiff base ligand (BBE) which is attached on the surface of $Fe_3O_4@SiO_2$/APTES. Weigh loss percentage at this step is about 8%.

The third step of weight loss has occurred in the range of 660–760˚C that can be related to the decomposition of the silica layer. The results of TGA showed the thin layer related to silica layer coating MNPs. From the tepmprature 790˚C onwards, no weight loss occurs. The total percentage of weight loss is approximately 15%.

3.1.3 VSM curve

VSM curves of Fe_3O_4 (a), Fe_3O_4@SiO_2 (b) and MSA-SB@Ni (II) are shown in Fig. 3. The magnetic properties of Fe_3O_4, Fe_3O_4@SiO_2 and Fe_3O_4@SiO_2 /APTES-Schiff base of Ni (II) (MSA-SB@Ni) were checked by vibrating sample magnetometry (VSM) at room temperature. The values of saturation magnetization (Ms) for MNPs, core-shell, Fe_3O_4@SiO_2 and attached nickel (II) Schiff base complexes on the surface of core-shell MNPs (MSA-SB@Ni) are 57, 42, and 30 emu/g respectivelly. As can be seen, the presence of silica and anchored nickel Schiff base complexes coating on magnetite nano-particles reduced the magnetic saturation values. It can be said that all three structures (Fe_3O_4, Fe_3O_4@SiO_2, and MSA-SB@Ni(II) are superparamagnetic because the curves show no obvious hysteresis loop and the remaining magnetization (Mr) and Hc values in MNPs and core-shell structures are very little. Decreasing the crystalline structre of MNPs by creating amorphous layers on them, probably lead to a reduce in magnetism saturation (Ms) of Fe_3O_4@SiO_2 and MSA-SB@Ni (II). Further, we can use a permanent simple magnet to separate, the nano-material from the solution of reaction without any problem. When the external magnet is removed, the catalyst disperses in the solution very quickly.

3.1.4 XRD-pattern

The XRD patterns of Fe_3O_4, Fe_3O_4@SiO_2 and nano-catalyst of MSA-SB@Ni have been shown in Fig. 4. The diffraction peaks at 2θ = 30.05˚, 35.65˚, 43.4˚, 54.3˚, 57.4˚and 63.6˚. These peaks are correspond to (220), (311), (400), (422), (511) and (440) Miller indices respectively. These patterns show that the magnetic core of Fe_3O_4 not affected by silica layer and functionalization by Schiff base complex. The broad diffraction peaks of XRD patterns of all three structures show that the structures are in nano-size. The XRD pattern of MNPs corresponds to reference with card no. (75 – 0033) and has cubic inverse spinel structure.

3.1.5 FE-SEM image

The morphology details and nano-particles size of the nano-catalyst was attained by Field Emission Scanning Electron Microscopy (FE-SEM) (Fig. 5). The FE-SEM image of MSA-SB@Ni indicate that the majority of nano-particle size of the novel nano-catalyst are around in the range of 60–65 nm and has the spherical morphologies with uniform particles in shape.

3.1.5.1 Particle size distribution histogram.

The particle size distribution histogram of nano-catalyst has been shown in Fig. 7. Two parameters, size (x-axis) and the number of particles (y-axis) observed. As can be seen, the smallest size is 20 nm and the

largest is 110 nm but the average diameter size of nano-catalyst estimated is about 65.5 ± 5 nm with high abundance

3.1.6 EDX-spectra

In order to obtain the elements of nano-catalyst sample, Energy Dispersive X Ray (EDX) analysis is a useful technique. EDX analysis of nano-catalyst has been shown in Fig.6.Based on the EDX results, which include the peaks of Fe (in the range of 6-7.2 kev and 0–1 kev) and O (in the range of 0–1 kev) elements related to magnetite, Si (in the range of 1–2 kev) and O elements related to silica coating, C and N (in the range of 0–1 kev), and Ni (in the range of 0-1 and 7–8 kev) elements related to the Schiff base complex, confirms that the Schiff base complex well functionalized on magnetite-silica nano-particles.

3.1.7 Leaching test of catalyst

The leaching test of catalyst shows that the presence of a catalyst in the preparation of a desired product in a desired reaction is very important and necessary. As can be seen, the absence of catalyst (blue line) reduces the efficiency of the product and much time does not help to improve the reaction in terms of yield. In the next experiment (green line), the catalyst was removed in the middle of the reaction with the magnet. As it's clear, the reaction efficiency did not improve with the catalyst leaving. While, in the third reaction (red line), only the presence of a small amount of catalyst could significantly increase the efficiency of the reaction.

3.1.9 AAS of nano-catalyst

In order to achieve to the amount of nickel (II) ion that involves in a certain amount of nano-catalyst, Atomic Absorption Spectroscopy (AAS) can help. In this way, a certain amount of compound (0.089 g of MSA-SB@Ni) was dissolved in aqua regia (HNO_3 + 3HCl) and volume reached to 120 mL. This solution used as an unknown solution to detect the amount of nickel (II) ion in the catalyst. Then some standard solution of nickel (II) nitrate was prepared (0.50 ,1.00, 1.50, 2.00, 2.50, 3.00, 3.50, 4.00, 4.50, 5.00 ppm). In the evaluation of the amount of nickel ion, was first diluted 1mL of the unknown solution with distilled water to a volume of 10 mL. Then the absorption intensity of the standard sample was measured by AAS. According to the device information and calculations, the concentration of the unknown sample, was about 4.4 ppm (0.092 mmole Ni in 0.089 g sample). This measurement shows that the nickel (II) ion forms a well-stable complex with Schiff base ligand (the active site of catalyst in 15 mg solid catalyst is 0.015 mole or 1.5% mole).

3.1.10 BET & BJH spectra

Porous materials are used extensively in chemical reactions from gas adsorption and using experimental data. The performance of a porous material as an internal specific surface area can be measured. Brunauer–Emmett–Teller (BET) theory is widely used to measure the specific surface area of a material. The main idea of special surface measurement goes back to Langmuir's single layer adsorption theory that later, this model was transformed into a multilayer adsorption model using BET theory. Today, it is used to determine the specific surface area of porous materials, including amorphous and crystalline

materials. Most solids have cavities inside their structures known as porosity is classified by their size, type, and shape. All the pores on a sample are called porosity, which is divided into two complete and useful (effective) forms. Effective or useful porosity consists of interconnected cavities that can drain fluids from within pass itself. Since the third type hysteresis does not show a limit on the uptake at high relative pressures, it has non-hard, plate-like, and incised cavities. The third type of hysteresis has a steep slope which leads to the closure of the loop, which is called the tensile strength effect. Using physical adsorption and correct analysis of the results obtained, we can find useful information such as specific surface area, porosity volume, and size distribution get the holes. Before getting the mentioned information, examining the isothermal curve gives us a relatively good understanding of the shape of the cavities. Finally using from the isotherm shape, the type of cavities in terms of micro, being meso or macro is almost obvious. This phenomenon occurs for nitrogen at a temperature of 77 K and a relative pressure between 0.4 and 0.45. (Fig. 9 shows the adsorption and desorption of MSA-SB@Ni).

This adsorption behavior is a description of mesoporous structure. By examining the type of adsorption and desorption spectra of our sample and comparing it with the six IUAPC spectra, we find that our sample is an H3-like hysteresis loop at high pressure. Since the desorption curve is P/P0 < 0.6 approximately related to the adsorption curve, it indicates that the holes are inclined towards the micro. The accumulation of nano-particles also resembled a sheet or plate and they are known as loose assemblages. Table 1 shows the surface physical characteristics of MSA-SB@Ni.

Particle pore distribution curves were performed according to the Barret- Joyner-Halenda (BJH) method. All samples were distributed in a similar and non-uniform mannerwith the center of these peaks in the mesoporous region (between 2–50 nm). These properties are very important because they demonstrate the availability of a catalyst surface to play a role in improving our amido-alkyl naphthol preparation targets.

3.2. Catalytic and substrate evaluation in the synthesis of amidoalkyl naphthol under thermal condition.

Table 2 shows Optimization and evaluation of nano-catalyst, reactants and reaction conditions. Table 3 shows model reaction and synthesis details of amido-alkyl naphthol derivatives in the presence of nano-catalyst in solvent free conditions. The prepared MSA-SB@Ni was used as a heterogeneous catalyst in the synthesis of amido alkyl naphthols. To optimize the preparation of amido-alkyl naphthol, various aldehydes, amides and 2-naphthol (fixed compounds) were used in the thermal conditions without solvent. First, at the temperature of 100 ° C, a suitable amount of catalyst was used to prepare the desired compound, which reached a final efficiency of 92% (Table 2, entry 1, 13). In the new experiment, at the same temperature, was reduced the amount of catalyst and was investigated the production reaction of amido-alkyl naphthol, which eventually reached 82% efficiency (Table 2, entry 2). In this part of the reaction, the amount of catalyst and temperature decreased, which led to a decrease in efficiency (Table 2, entry 3). In the fourth part, the temperature reached 70 ° C, but the amount of catalyst was not reduced, which also reduced the efficiency (Table 2, entry 4). Amidoalkyle naphthols can be prepared with almost

any aldehyde but, electron donor groups such as CH_3, OH, etc, on the aldehyde are not suitable because the transition state of amido alkyl-2-naphthol is unstable and the production of product has a low efficiency (Table 2, entry 5, 6, 9). The electron withdrawing groups on the aldehyde such as NO_2, Cl is very suitable for this process because it makes the higher efficiency for production (Table 2, entry 7, 8). The efficiency percentage is about 95 and the reaction time is limited and this is a very important issue for the synthesis of amido alkyl naphthols. Our novel catalyst is very good for this reaction. Despite the adequate amount of catalyst, temperature, and time, the use of Cu, Mn and Zn catalyst type (MSA-SB@Cu, MSA-SB@Mn, and MSA-SB@Zn) could not increase the production efficiency (Table 2, entry 10, 11, 12). at the last stage of the experiment, the type of catalyst and its amount as well as the temperature were appropriate, but we reduced the reaction time, which ultimately reduces the efficiency (Table 2, entry 14, 15). In summary, the whole Table 2 shows the importance of the type of catalyst, its amount, temperature, and time in preparation of amido alkyl naphthol.

The optimization of the amount of nano-catalyst (% mol toward reactants) based on the various experiments has been shown in Fig. 11.

3.3.Comparison of the catalytic efficiency of MSA-SB@Ni nano-catalyst with other reported catalytic systems

In order to show the merit of our novel nano-catalyst efficiency in comparison with some other nano-catalyst reported in the literatures, the results of our work has been compared with some other works. Table 4 shows comparison of nano-catalyst efficiency was used in this work with other reported catalysts that used for synthesis of amido-alkyl naphthol. Table 4 obviously shows that the novel MSA-SB@Ni nano-catalyst with a magnetic core, is one of the most efficient nano-catalysts for the synthesis of amido-alkyl naphthols.

3.4. The mechanism synthesis of amidoalkyl-2-naphthol

A tentative proposed mechanism for the synthesis of amido-alkyl naphthols has been shown in Scheme 3. R_1 is the derivation of aldehyde and R_2 is the derivation of amide. These compounds were mixed with β-naphthol (fix compound) to synthesis 1-amidoalkyl-2-naphthol. First, the novel nano-catalyst attached to the oxygen of benzaldehyde and activates the carbon (lone pair electrons of oxygen is nucleophile) (step 1). Second, the lone pair electrons of hydroxyl in β-naphthol poured to the vicinal ring of β-naphthol (step 2) and its π bond (as a nucleophile) attacks to the activated carbon of aldehyde (step 3). Next, electron resonates into the bond between metal in catalyst and oxygen in carbonyl (step 4). Later H_2O molecule leaves the compound (step 5–7). At the next step new π bond formed in aliphatic carbon near the aromatic ring. Then the lone pair electron of the nitrogen from amide attacks the aliphatic carbon (step 8). Then the π bond resonance to the ring and the aromatic ring formed again (step 9–10). Finally, the addition of hydrogen is the last step for the synthesis of amidoalkyl-2-naphthol (step 11). At the end the catalyst separated from reaction by an external magnet (step 12). The mechanism synthesis of 1-amidoalkyl-2-naphthol has been shown in scheme 3.

3.5. Reusability of catalyst

The reusability of a catalyst is an important factor of that catalyst in the point view of its industrial use. MSA-SB@Ni has used as catalyst five times in different reactions for the synthesis of amido alkyl-2-naphthol derivatives as shown in Fig. 12. As can be seen, the yield amount of catalyst in the first and second reaction was 95% but in the third, fourth, and fifth reactions the yield were 92%, 89%, and 87% respectively. It revealed almost no loss of activity after five run of reaction thus the reusability of the catalyst was very successful with this evidence. The catalyst was separated with a simple magnet and washed with ethanol and water for every reaction.

3.6. Investigation of the structure of nanocatalysts after participating in several processes.

According to the identification and analysis of nano-catalyst by XRD and FE-SEM techniques after use as catalyst (Fig. 13), we concluded that the crystal structure of the catalyst after participation in the production process of the amido alkyl-naphthol has not changed and the particle size and morphology are preserved. But it makes sense to say probably a small part of active sites of nano-catalyst has been contaminated.

4 Conclusions

This work has established and explained that the novel catalyst MSA-SB@Ni is the efficient and reusable heterogeneous catalyst for the green synthesis of 1-amidoalkyl-2-naphthols. The active site of the catalyst is a nickel (II) Schiff base. First an aliphatic $-N_2O_2$ tetra-dentate Schiff base was synthesized separately and successfully functionalized on magnetite silica. Then this tetra-dentate Schiff base functionalized on magnetite core metalated by nickel (II). The aliphatic Schiff basses less used as catalyst because of the aliphatic metal Schiff bases are prone to polymerization. Functionalization of aliphatic Schiff base on a magnetite silica core-shell prevents polymerization and metal Schiff base can be used as an efficient catalyst without any worries. The nano-catalyst was extracted easily by an external magnet. Also in this article, the prepared nano-catalyst fully characterized with some techniques such as FT-IR, XRD, TGA, VSM, EDX, FE-SEM, AAS, and BET. Synthesis of 1-amidoalkyl-2-naphthol with aldehyde, β-naphthol and amide and a small amount of MSA-SB@Ni as catalyst was characterized with TLC, FT-IR, and ^{1}HNMR. All of the information about amidoalkyl-2-naphthol derivation has been shown in Table 4. This catalyst has an important role in the synthesis of any organic component because does not have any trouble for reaction and is separated very easily.

Declarations

Conflict of Interest:

The authors declare that they have no conflict of interest.

Funding:

This study was funded by University of Kashan

Acknowledgements

The authors are grateful to University of Kashan for supporting this work

References

1. B. Asadi, I. Mohammadpoor, S. Tangestaninejad, M. Moghadam, V.Mirkhani and A. Landarani-Isfahani, New J. Chem. **40**, 6171 (2016)
2. X. Li, S. Zhang, B. Yang, C. Lv, X.Jia and Z. Hu, RSC Adv., 2016, 6, 86531-(2016
3. G. Mohammadi Ziarani, M. Malmir, N. Lashgari, A. Badiei, RSC Adv. **9**, 25094 (2019)
4. K. Ji-Eun, J.Young Shin, M. Cho, Arch. Toxicol. **86**, 685 (2012)
5. Z. J.Qu, Q. Tian, Wang,, Q. Zhou, J. Lin, Si. Peng, Jian-bin Luo. RSC Adv. **8**, 35437 (2018)
6. S. Karimi, H. Namazi, New J. Chem. **45**, 6397 (2021)
7. A. Sajjadi, R. Mohammadi, J. Med. Chem. Sci. **2**, 55 (2019)
8. QiLong Zhu, Q. Xu, Chem. **1**, 220 (2016)
9. J. Liu, H. Qiu, F. Zhang, Y. Li, New J. Chem. **44**, 5324 (2020)
10. S. Karami, M.G. Dekamin, E. Valiey, P. Shakib, New J. Chem. **44**, 13952 (2020)
11. S. Maria, M. Georgescu, L. Alexandrescu, D. Gurau, A. Ficai, D. Ficai, E. Andronescu, Curr. Pharm. Des. **21**, 5324 (2015)
12. M. Langeroudi, M. Pourabhari, and E. Binaeian. Mater. Chem.Phys., 210 (2018)
13. H. Rajabi, H. Arjmand, S. Jafar, Hoseini, H. Nasrabadi, Magn. Magn. Mater. **394**, 7 (2015)
14. A. Behbahani, N. Sadati, K. Rostamizadeh, M.R. Yaftian, A. Zamani, H. Ahmadi, J. Environ. Health. Sci. **12**, 1 (2014)
15. A. Araghi, S. Hozhabr, M.H. Entezari, Appl. Surf. Sci. **333**, 68 (2015)
16. M. Asadi, M. Setoodehkhah, A.H. Kianfar, J. Iran. Chem. Soc. **7**, 38 (2010)
17. L. Xiang, **and** J. René, Hamon. Coord. Chem. Rev. **389**, 94 **(** (2019), **)**
18. K.C. Gupta, A.K. Sutar, Coord. Chem. Rev. **252**, 1420 (2008)
19. M.T.ümer,Ç Cumali, H. Köksal, **and** S. Selahattin, Transit. Met. Chem. **24**, 525 **(** (1999), , **)**
20. G. Mohamed, A.A. Spectrochim, Mol. Biomol. Spectrosc. **64**, 188 **(** (2006), **)**
21. N. Kocak, M. Sahin, G. Arslan, H.I. Ucan, J. Inorg. Organomet. Polym. **22**, 166 (2012)
22. D. Kara, A. Fisher, S.J. Hill, J. Hazard. Mater. **165**, 1165 (2009)
23. M. setoodehkhah, S. Momeni, J. Inorg. Organomet. Polym. **28**, 1098 (2018)

24. A. Afkhami, T. Madrakian, R. Ahmadi, H. Bagheri, M. Tabatabaee, Microchim. Acta **175**, 69 (2011)
25. H.R. Shaterian, H. Yarahmadi, Tetrahedron Letters. **49**, 1297 (2008)
26. A.R. Hajipour, Y. Ghayeb, N. Sheikhan, A.E. Ruoho, Tetrahedron Letters. **50**, 5649 (2009)
27. A.E. Rosamilia, C.R. Strauss, **and** J. L. Scott. Pure, Appl. Chem. **79**, 1869 **(** (2007), , **)**
28. S. Rajesh, R. Bala, R. Duvedi, **and** S. Kumar, Iran. J. Catal. **5**, 187 **(** (2015), , **)**
29. H.R. Shaterian, A. Amirzadeh, F. Khorami, M. Ghashang, Synth. Commun. **38**, 2983 (2008)
30. N. Ganesh Chandra, S. Samai, R. Kumar, M.S. Singh, Tetrahedron. Letters. **50**, 7220 (2009)
31. B. Baghernejad, E. Ashoori. J. appl. chem. Res. **14**, 22 **(** (2021), , **)**
32. D. Afinisha, J. Viswanadhan, Orient. J. Chem. **33**, 1354 (2017)
33. H. Kiyani, H. Darbandi, A. Mosallanezhad, F. Ghorbani, Res. Chem. Intermed. **4**, 7561 (2015)
34. R. Ghorbani-Vaghei, S. Malaekehpour, Open Chem. J. **8**, 1086 (2010)
35. D. Biswanath, C.R. Reddy, J. Kashanna, S. K.Mamidyala, and C.G. Kumar, Med. Chem. Res. **21**, 3321 (2012)
36. B. Khawla, H. Boulebd, C. Bensouici, D. Harakat, R. Boulcina, A. Debache, Chemistry. Select. **5**, 5515 (2020)
37. B. Bananezhad, M.R. Islami, H. Khabazzadeh, J. Iran. Chem. Soc. **16**, 865 (2019)
38. W. Min, Z. Song, Y. Liang, Org. Prep. Proced. Int. **43**, 484 (2011)
39. B. Maleki, F. Taimazi, Org. Prep. Proced. Int. **46**, 252 (2014)
40. N. Lingaiah, M. Baseeruddin, S. Apuri, S. Kantevari, Catal. Commun. **8**, 1729 (2007)
41. S.A. Ansari, M.K. Jaiprakash, N. Sangshetti, N.D. Kokare, P.S. Wakte, D.B. Shinde, Ind. J. Chem. Technol. **17**, 71 (2010)
42. R. Tayebee, M. Amini, M. Akbari, A. Aliakbari, Dalton Transactions. **44**, 9596 (2015)
43. L. Nagarapu, M. Baseeruddin, S. Apuri, S. Kantevari, Indian J. Chem. Technol. **312**, 53 (2007)
44. H.R. Shaterian, H. Yarahmadi, M. Ghashang, Tetrahedron. **64**, 1263 (2008)
45. M. Dehbashi, M. Aliahmad, M. Shafiee, M. Ghashang, Inorg. Nano-Met. Chem. **43**, 1301 (2013)

Tables

Due to technical limitations, table 1 to 4 is only available as a download in the Supplemental Files section.

Figures

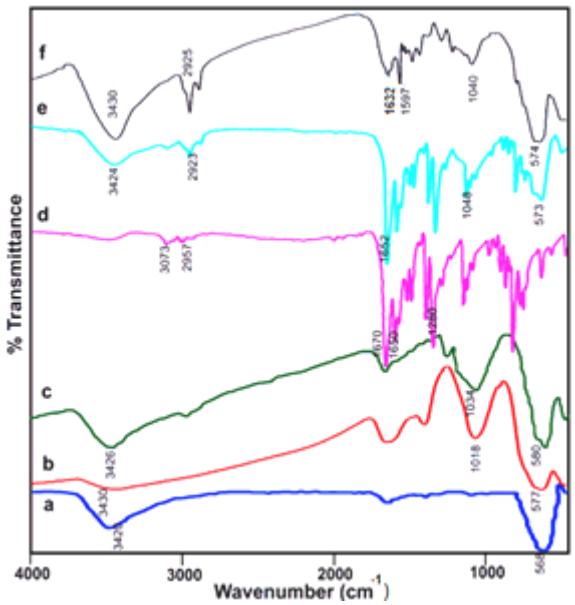

Figure 1

FT-IR spectra of FT-IR spectra of Fe3O4 (MNPs) (a), Fe3O4@SiO2 (b), Fe3O4@SiO2/APTES (c), Schiff hase (BBE) (d), Fe3O4@SiO2/Schiff base (e) and MSA-SB@Ni (II) (f)

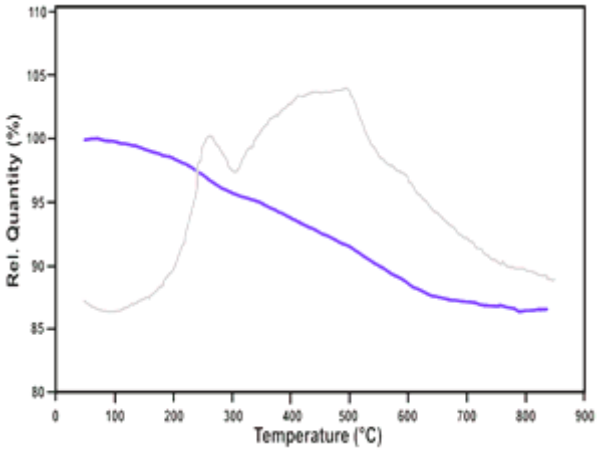

Figure 2

TGA curve of MSA-SB@Ni (II)

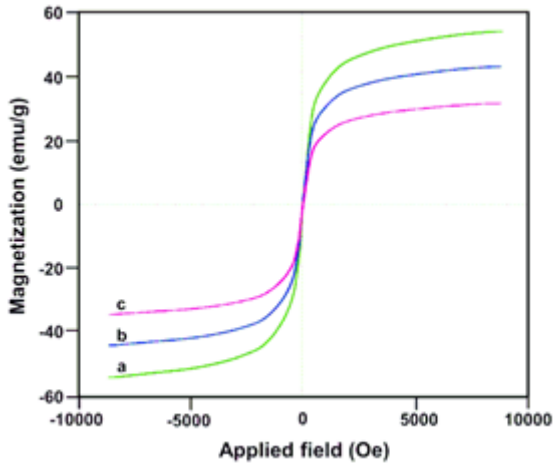

Figure 3

VSM curves of Fe3O4 (a), Fe3O4@SiO2 (b) and MSA-SB@Ni (c)

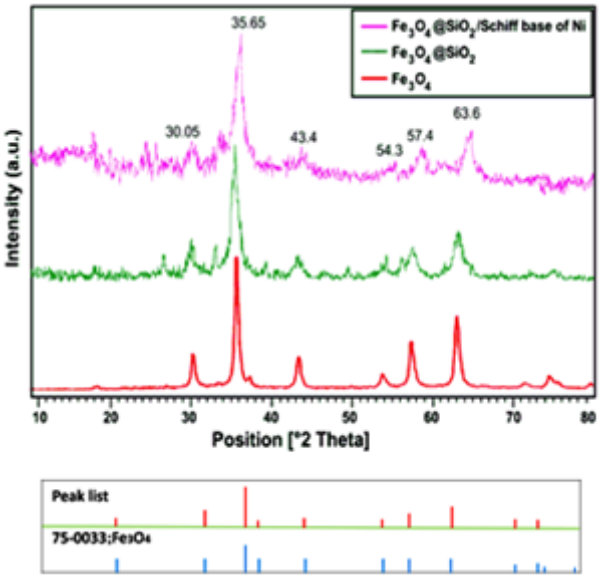

Figure 4

XRD of Fe3O4 , Fe3O4@SiO2, MSA-SB@Ni

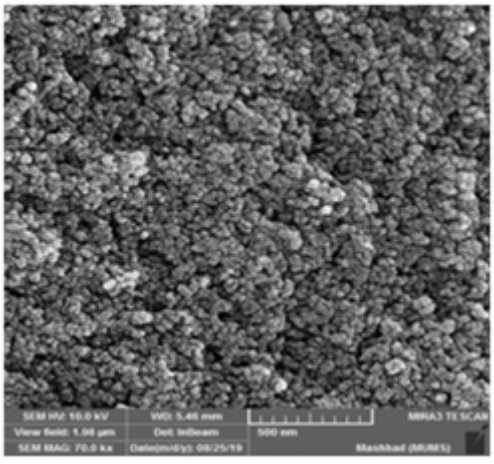

Figure 5

The FE-SEM image of MSA-SB@Ni

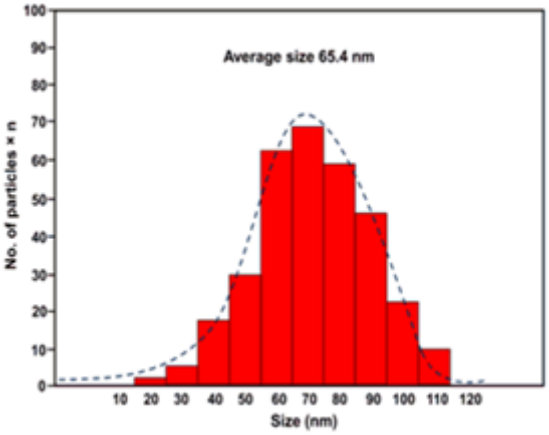

Figure 6

Particle size histogram of catalyst (MSA-SB@Ni)

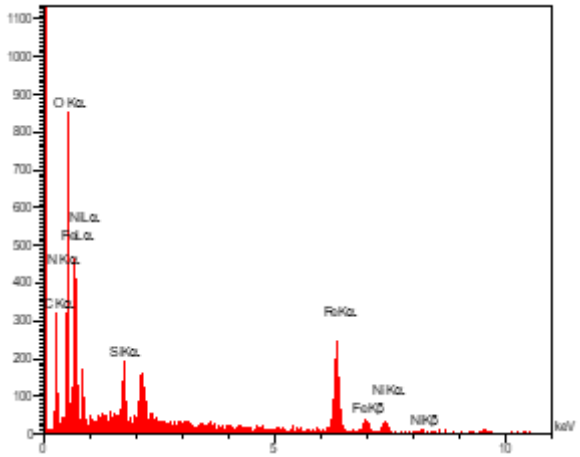

Figure 7

EDX Spectrum of MSA-SB@Ni

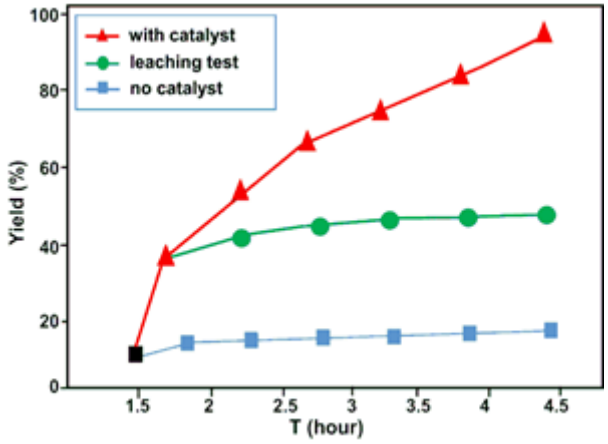

Figure 8

Leaching test of catalyst, (MSA-SB@Ni)

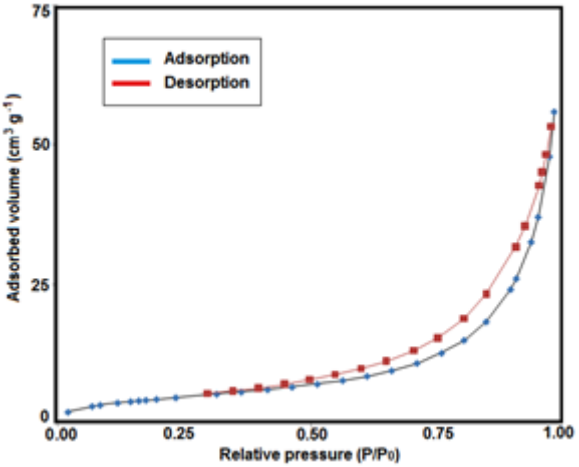

Figure 9

Nitrogen adsorption/desorption isotherms of MSA-SB@Ni

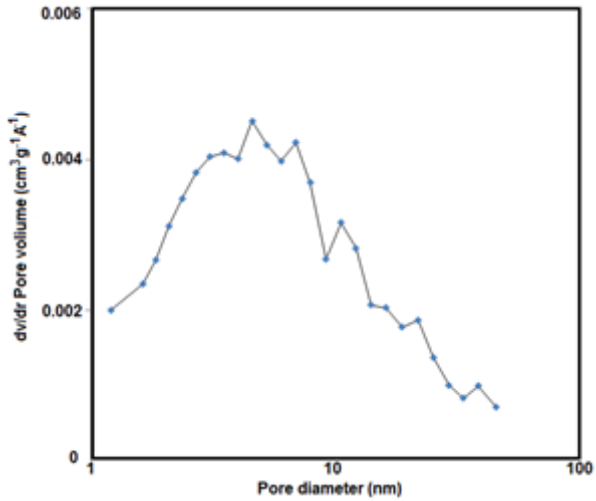

Figure 10

Barret-Joyner- Halenda (BJH) pore size distributions plots of MSA-SB@Ni

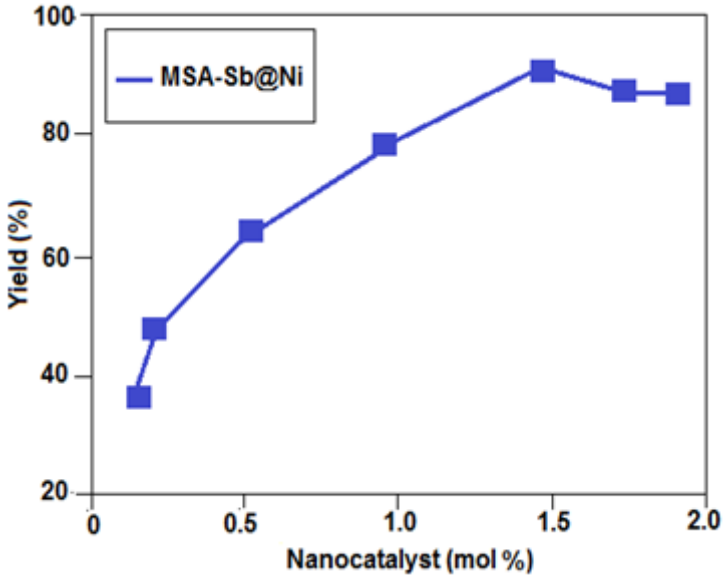

Figure 11

The optimaation of the amount of nanocatalyst (mol %)

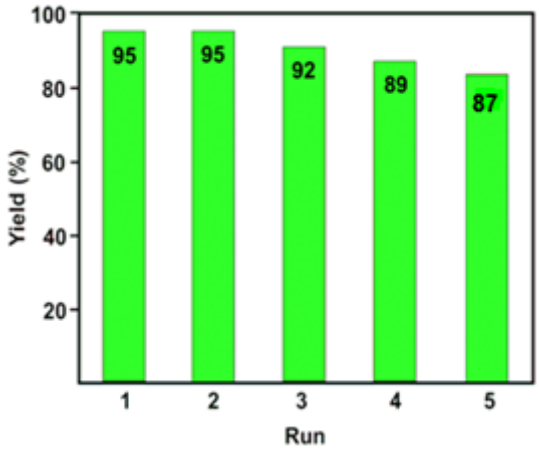

Figure 12

Reusability of catalyst MSA-SB@Ni in reactions

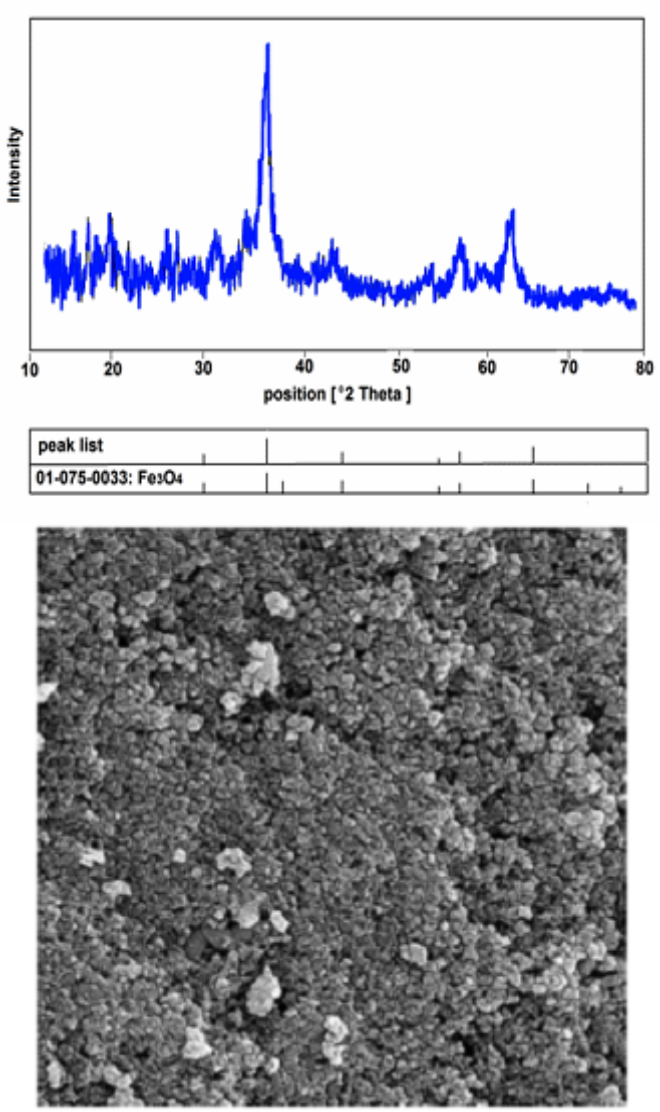

Figure 13

FE-SEM and XRD pattern of nano-catalyst after using

Supplementary Files

This is a list of supplementary files associated with this preprint. Click to download.

- Tables.docx
- Scheme01.png
- Scheme02.png
- Scheme03.png